

# "Preparation of SnO<sub>2</sub> thin films by doping with F<sup>-1</sup> ions using chemical spray pyrolysis"

Abdulsamee Fawzi Abdul Aziz Albayati

Physics Department , College of Education and Pure Sciences , Tikrit University , Tikrit , Iraq

Email: [abdulsamee\\_fawzi@yahoo.com](mailto:abdulsamee_fawzi@yahoo.com)

## Abstract

In this paper, the structural and optical properties of pure Tin Oxide and doped by Fluorine (F). Thin films were studied prepared by chemical spray pyrolysis on glass substrates at temperature 400°C. The nature of crystallization of the compounds was examined by using X-Ray diffraction technique which showed that the prepared thin films are polycrystalline structure, and the doping processes didn't show any obvious differences on the crystalline structure of (SnO<sub>2</sub>). The DC conductivity measurements of the samples were performed by means of a two probe method. The activation energies were computed from the plots of  $\sigma_{dc}$  versus 1000/T. To obtain the optical parameters, the absorption and transmittance spectra were recorded in the wave length range 300-1100 nm, the energy gap of the direct and indirect allowed transition were calculated. The optical parameters such as absorption coefficient ( $\alpha$ ), refractive index (n), extinction coefficient ( $K_o$ ), dielectric constant ( $\epsilon'$ ), and dielectric loss (tan $\delta$ ), were also investigated.

**Keywords:** SnO<sub>2</sub>; F thin film; chemical spray pyrolysis; XRD analysis; optical properties

## 1- Introduction

Fluorine-doped tin oxide (FTO) film is widely used for optoelectronic applications such as displays, solar cells, light emitting diodes, smart windows, etc. [1]. Compared to indium-doped tin oxide (ITO), FTO has many advantages such as low cost, chemical resistance, and high availability of precursor sources [2]. In addition, ITO suffered from low electrical conductivity after annealing treatment in an oxygen atmosphere during fabrication of dye-sensitized solar cells (DSSCs) [3,4]. This case was not found in the application of FTO as electrodes for DSSCs. Therefore, FTO would be an economically viable and a best candidate for DSSCs electrodes. The fabrication of FTO thin films has been reported by various methods, which includes spray pyrolysis deposition (SPD), sputtering, and chemical vapor deposition and thermal evaporation method [5-9]. The SPD method is the most popular due to its simplicity, low cost, and scale-up ease [10-11]. Several modifications of the SPD method have been reported, such as the application of lamp radiation for a substrate heater [12], electric field induction [15], and the use of an ultrasonic nebulizer as a droplet generator [16]. Several materials have been fabricated using spray pyrolysis deposition method, such as SnO<sub>2</sub>:F/CdS [17], TiO<sub>2</sub> [18] and yttria-stabilized zirconia [19].

In this work, we present an analysis of the effect of F<sup>-1</sup> doping to polycrystalline SnO<sub>2</sub> thin films deposited chemical spray pyrolysis route with several concentrations of F<sup>-1</sup> (1, 2, 3, 4 and 5%) on their electrical and optical properties.

## 2. Experimental details

SnO<sub>2</sub> films doped with F were prepared by the spray pyrolysis technique to employ as window in the thin film solar cells. The spray solution is containing stannic chloride (SnCl<sub>4</sub>.5H<sub>2</sub>O), methanol and H<sub>2</sub>O. In order to dope F into the SnO<sub>2</sub> films, HF was used as a source. The atomic ratio of F/Sn was varied from 0.01 to 0.05 in the solution. The solution was sprayed

on to the substrates held at temperature of 400 C. The substrate temperature was optimized to obtain quality films, which was reported in the literature. The spray rate was kept to be 5 ml/min. The compressed air was used as the carrier gas. The details of deposition process of SnO<sub>2</sub> films are given elsewhere [20]. X-ray diffract meter (model Bruker D8 Advance), having Cu-K $\alpha$  radiations of wavelength,  $\lambda = 1.5418 \text{ \AA}$  was used to record X-ray diffraction patterns of the samples. Electrical characteristics of the films were studied by the standard two-probe method using a Keithley multimeter (Model 2000). The transmission and absorption spectra of the doped and undoped thin oxide films in the visible region has been recorded using UV-Visible spectrophotometer model (GBC scientific Equipment). All the spectra have been recorded by placing a blank substrate in the reference beam of the instrument. A computer program was employed to obtain the optical constants, absorption coefficient, and electron transitions.

## 3 Results and discussion

### 3. 1 Structural analysis by XRD

The XRD patterns of SnO<sub>2</sub> with various F contents calcined at 450 °C are shown in Fig. 1 All the patterns were indexed using the database Joint Committee on Powder Diffraction Standards (JCPDS) data for pure SnO<sub>2</sub> card no. (46-1088), which depict tetragonal perovskite structure of all samples. There are no extra peaks indicating purity of the samples synthesized. The positions of all the Bragg lines were used to obtain the interplaner spacing and these values were used to index the peaks. The observed and calculated d' values for plans are given in Table 1.

**Table 1 – Miller indices and interplaner spacing for SnO<sub>2</sub> thin film**

(hkl)	d <sub>obs.</sub>	d <sub>cal.</sub>
(110)	3.35	3.351
(100)	2.998	2.995
(211)	2.793	2.789
(101)	2.647	2.651
(101)	2.517	2.513
(200)	2.379	2.379
(211)	1.763	1.764
(111)	1.498	1.501
(210)	1.417	1.419
(201)	1.313	1.301
(112)	1.297	1.293

The lattice parameters  $a=b= 4.739\text{Å}$ ,  $c = 3.193\text{Å}$  ( $c/a= 0.673$ ) and unit cell volume =  $72.15 \text{Å}^3$  are in good agreement with the earlier reports [21]. On F<sup>-1</sup> doping the intensity of all peaks were decreased. On increasing the concentration of (F<sup>-1</sup>) the intensity of the SnO<sub>2</sub> peaks were further decreased due the decrease in the atomic density in these planes. The decrease in peak intensities is basically due to the replacement of Sn<sup>+4</sup> ions with F<sup>-1</sup> ions in the lattice of SnO<sub>2</sub> as in [22]. This process leads to the movement of Sn<sup>+4</sup> ions in the interstitial sites and also an increase in the amorphous phase and disorder. The XRD pattern of SnO<sub>2</sub> films doped at different concentration of F is given in Fig. 1.

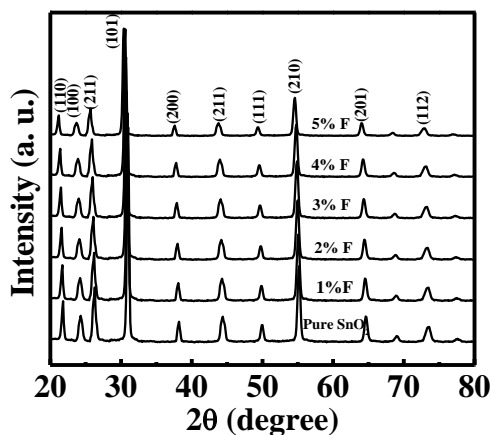


**Fig. 1 The XRD patterns of SnO<sub>2</sub> with various F contents**

The average crystallite size (D) values were determined from (101) plane peak with using Scherer’s formula [23-24]:

$$D_p = \frac{k\lambda}{\beta \cos \theta} \dots(1)$$

where  $\beta$  is the full-width half-maxima (FWHM) of the XRD peaks, D is the particle size,  $\lambda$  is the wave length of x-ray radiation =  $1.5418\text{Å}$ ,  $K = 0.9$  (assuming the particles are spherical in shape),  $\theta$  is the Bragg angle.

The average crystallite size is found to be ~ 85nm. Two molecules of SnO<sub>2</sub> contain two tin atoms and four oxygen atoms per unit cell with tetragonal (rutile) structure. The bond length  $D_n = R_A + R_B + D_N$

=  $2.11 \text{Å}$  where  $R_A$  and  $R_B$  are ionic radii of Sn and O<sup>-2</sup> respectively and  $D_N$  is a correction factor for coordination number (6) which is 0. The estimated bond length is little bit higher than the observed value of 2.053 and 2.057 Å. This difference could be due to the contribution of the covalent forces to the crystal bonding (i.e., partly covalent bonding or not totally ionic) [25]. The Sn atom is located at the centre of the unit cell i.e., the cell has body centered tetragonal structure. Each Sn atom is surrounded by six oxygen atoms in a slightly distorted octahedral coordinatic. Each oxygen atom is surrounded by three Sn atoms at the corners of an almost equilateral triangle. In other fashion, in alternate diagonals of planes, two oxygen atoms are situated between consecutive Sn atoms [26].

**3.2. DC conductivity**

The DC conductivity for all the samples was measured by the two probes method in a temperature range from 300 to 500K. The measured DC conductivity of the samples at room temper sure was found to vary from  $4.7 \cdot 10^{-3}$  to  $5.6 \cdot 10^{-4} (\text{cm} \cdot \Omega)^{-1}$ . The resistivity  $\rho$ , measured by using equation (2).

$$\rho_{dc} = \frac{RA}{t} \dots (2)$$

Where, (R) is the ohmic resistance of the sample, (A) is the cross section area film sheet and (t) is the conductor length (inter electrode spacing). The variation of  $(\ln \sigma_{d,c})$  values with  $10^3/T$  for all samples are plotted in Fig . 2 . It has been noticed from the same figure that the electrical conductivity increases exponentially as the temperature increases .This represents a common semiconductor properties, which is related to increasing the charge carrier's concentration with temperatures. The electrical activation energy obtained by fitting the DC conductivity data with Arrhenius relation (3).

$$\sigma = \sigma_o \exp\left(\frac{-\Delta E}{kT}\right) \dots(3)$$

$\Delta E$  is the activation energy and interpreted as the energy required to cause the electron jump as referred above, k is Boltzman constant and T is the absolute temperature. The results of  $\Delta E$  was found to vary from  $4.7 \cdot 10^{-3}$  to  $5.6 \cdot 10^{-4} \text{eV}$ .

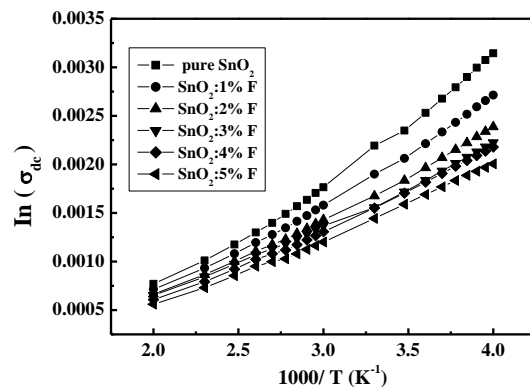


**Fig (2) Variation of DC conductivity with temperature for pure and doped samples.**

3.3 Optical properties

3.3.1 Absorptivity

Fig. 3 shows that the absorptance of the film decreases gradually at low energies this change is due to the low absorptance of the photons which has lower energies than that of the film. The absorptance increases rapidly at high energies (short wave lengths) corresponding to the energy gap of the film, (when the incident photon has an energy equaling or bigger than the energy gap value).

This evident increase is due to the interaction of the material electrons with the incident photons which have enough energy for the occurrence of electron transitions. Increasing the doping percentage increases lead to increasing the absorptance, this attribute to increases the energy gap of the film.

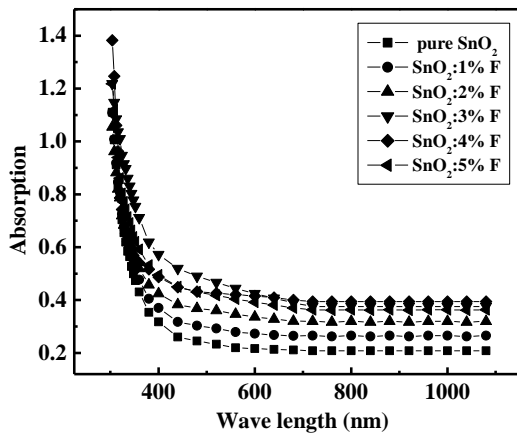


Fig 3 Absorption versus wave length for pure and doped samples

3.3.2 Transmittance

The transmittance (T) spectra of F-SnO<sub>2</sub> (1%, 2%, 3%, 4% and 5%) thin films as a function of wavelength ranging from 300 to 1100 nm is shown in Fig. 4. The transmittance value is found to decrease gradually if the antimony concentration is increased above 5%. Doping rate. Measurements of Transmittance are according to equation (3) [27]:

$$\alpha = \text{Ln} (T_1/T_2) / (t_2-t_1) \dots (4)$$

Where,  $t_1, t_2$  : are the thicknesses of first and second film .

$\alpha$  : Absorption coefficient,  $T_1, T_2$  : Transmittance of first and second films .

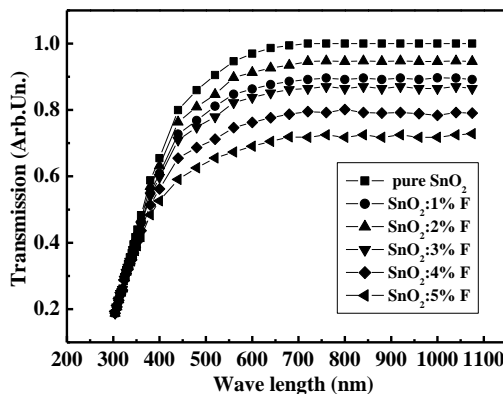


Fig .4 Transmittance versus wave length for pure and doped samples

3.3.3 Reflectivity

Reflectance was calculated using equation [28]:

$$R + T + A = 1 \dots (5)$$

Fig.(5) shows the reflectivity of the undoped and doped tin oxide. it is clearly seen from this fig. that reflectivity increases slightly with doping percentage

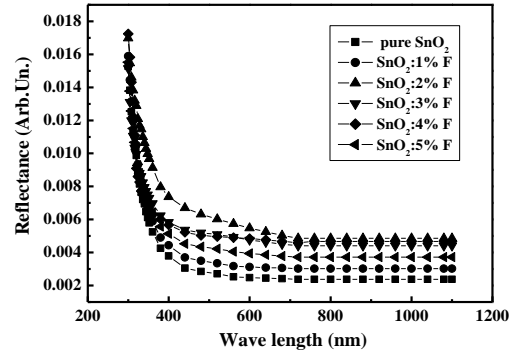


Fig .5 Reflectance versus wave length for pure and doped samples

3.3.3 Absorption Coefficient

The absorption coefficient was calculated using the equation [28].

$$\alpha = \left( \frac{2.303A}{t} \right) \dots (6)$$

Where,  $\alpha$ : photo absorption coefficient which changes with the incident wave length upon the material,  $t$  : the thickness of film .  $A$ : Absorption  
 Fig.(5) shows the relation between absorption coefficient and photon energy for all the samples. It is clearly seen that the absorption edge is not sharp and this may be related to the polycrystalline structure of thin films. The increase in  $\alpha$ , observed on high-energy side of the spectra ( $>3$  eV) can be associated with the band-to- band transition. The observed absorption edge lies at 3.5 eV for undoped tin oxide and on doping it shift toward higher energies, which is due to Moss-Burstein effect [29]. Note that the absorption edge increase with doping except for 2% for which the absorption edge is below the undoped sample. This might be due to impurities that essentially exist in the undoped film as a result for spraying process in air ( $O_2, N_2, H_2$ ). We notice that 2 % doping is enough to exist the thermodynamic equilibrium. [30]. Since the value of  $\alpha$  is in the order of  $10^6 \text{ m}^{-1}$  and the absorption coefficient is measured at room temperature, the presence of exaction bands is not likely to be possible. Therefore, the absorption is from band to band transition, which suggests the occurrence of direct allowed and forbidden transition [31]. Results of Urbach tails confirmed the results of optical gap, where  $E_u$  was found to have the same values within the plot Variation of absorption coefficient with photo energy for all the considered films [32].

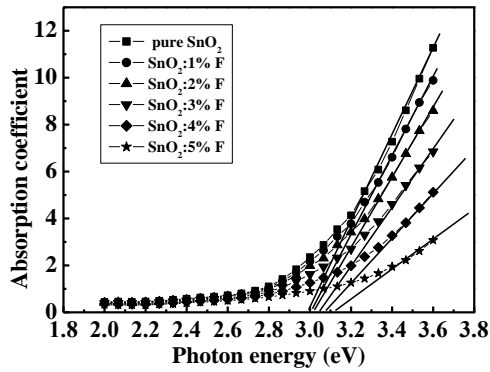


Fig (6) Absorption coefficient versus photon energy for pure and doped samples

3 – 3 - 4 Direct Allowed Transition

The direct allowed energy gap was determined by plotting  $(\alpha h\nu)^2$  as a function of photon energy  $(h\nu)$  and were shown in Fig.(6), the band gap energy ( $E_g$ ) was determined by extrapolation of the straight line region of the plots  $(\alpha h\nu)^2$  versus photon energy  $(h\nu)$ . The direct band gap was found to increase from  $(3.5 - 3.54)$  eV with increasing doping percentage. The increase in band gap can be attributed to the Burstien-Moss shift.

The following formula clarifies such transition [33]:

$$\alpha h\nu = A(h\nu - E_g)^r \dots\dots(7)$$

Where ,  $\alpha$  : Absorption coefficient,  $h\nu$  : Absorbed photon energy.

$E_g$  : forbidden Energy gap, A : constant , r : exponent coefficient its value depends on the quantity of transition.

If (r) equals (1/2) , transition is being direct allowed transition but if it is (3/2) it is direct forbidden transition in which transition is from nearby areas to direct allowed transition ones without change in the value of wave vector (k) . we observe that both the two transitions do not depend on temperature degree . [34].

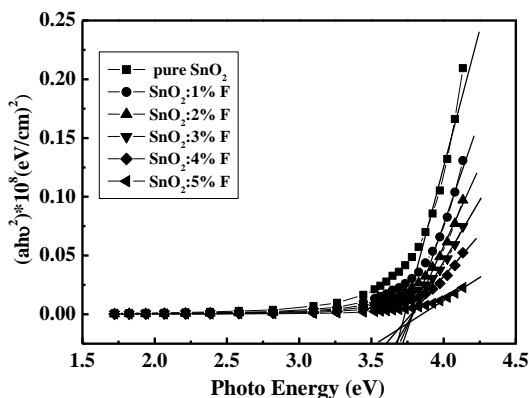


Fig. (7) Direct Allowed Transition versus photo energy for pure and doped samples.

3 – 3 - 5 Extinction Coefficient

The extinction coefficient ( $k_0$ ) was calculated using the relation [33]

$$K_o = \frac{\alpha\lambda}{4\pi} \dots\dots(8)$$

Fig. (8) shows the variation of extinction coefficient as a function of photon energy for all the doped and undoped tin oxide samples. it is obviously seen that  $k_0$  increases approximately exponentially with photon energy and then increases rapidly in the high photon energy. The data of  $k_0$  shows that the value increased as the doping increased,  $K_0$  increased very slightly as a function of photon energy in the low photon energy range and increased rapidly in the high photon energy range, and as the doping percentage increased, the shape of the curve at low photon energy became almost linear especially in the 2 % doping percentage. Similar behaviors were reported earlier by Khalid [35].

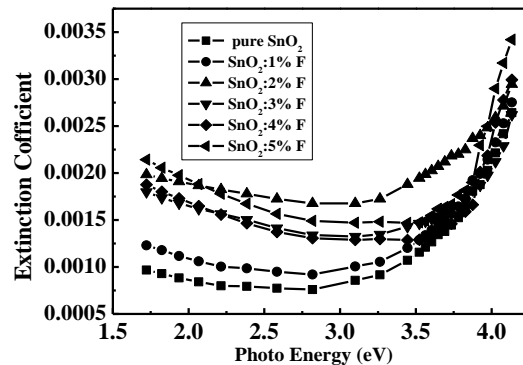


Fig. 8 Variation of extinction coefficient with photo energy for pure and doped samples.

3-3-6 Refractive Index

Refractive index was calculated by means of equation [33]:

$$n_o = \left[ \frac{(1+R)^2}{(1-R)^2} - (K_o - 1) \right]^{1/2} + \frac{(1+R)}{(1-R)} \dots\dots (9)$$

In fig. (4-8), the refractive index versus photon energy is plotted as a function of doping percentage. refractive index increased as the doping percentage increased. Xu et al [36 ] have also indicated that refractive index increases on increasing of the  $F^{-1}$  percentage.

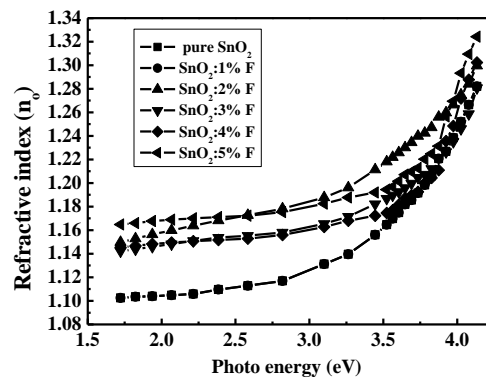


Fig. 9 Variation of Refractive index with photo energy for pure and doped samples.

3-3-7 Dielectric measurements

Real and imaginary part of dielectric constant were calculated using the equations (10) and (11) respectively [33].

$$\epsilon_1 = n_o^2 - k_o^2 \dots\dots(10)$$

This relation represents real dielectrical constant while imaginary dielectrical constant is written as follows :

$$\epsilon_2 = 2 n_o k_o \dots\dots(11)$$

Figs. (10) and (11) show the plots of real and imaginary parts of the undoped and doped samples. All the samples behave like the refractive index samples which means that the real and imaginary parts increased as the doping percentage increased. Similar behaviors were reported earlier by Ziad et. al. [36].

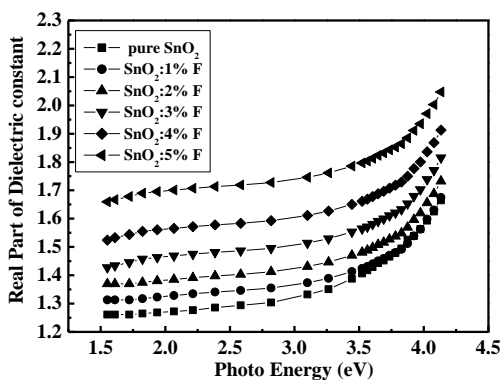


Fig. 10 Variation of Real part of dielectric with photo energy for pure and doped samples.

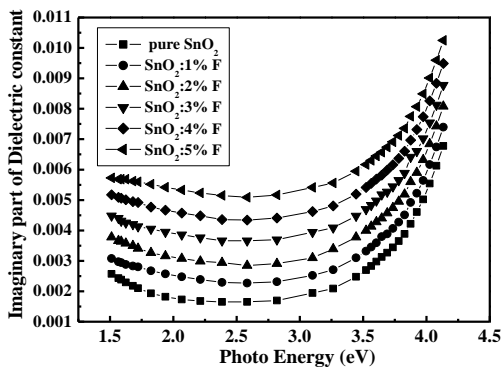


Fig. 11 Variation of imaginary part of dielectric with photo energy for pure and doped samples.

The dielectric loss is obtained from the data of ac conductivity was calculated by using the formula [37].

$$\sigma_{ac} = \omega \epsilon_1 \epsilon_o \tan \delta \dots\dots(12)$$

Fig. (12) owns the variation of dielectric loss with photo energy for pure and doped samples. It can be seen that (tan δ) increases with increasing of F-concentration for films at room. This may be related to the fact that, at increasing F-concentration the loss is dominated by thermally activated electron hopping.

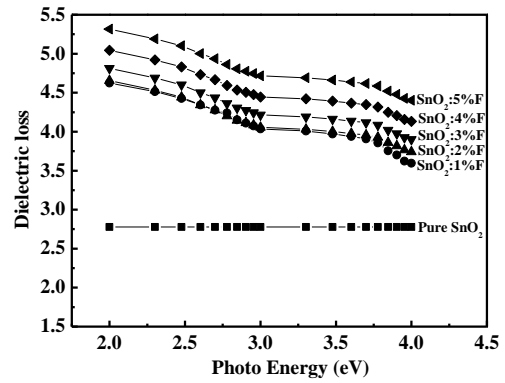


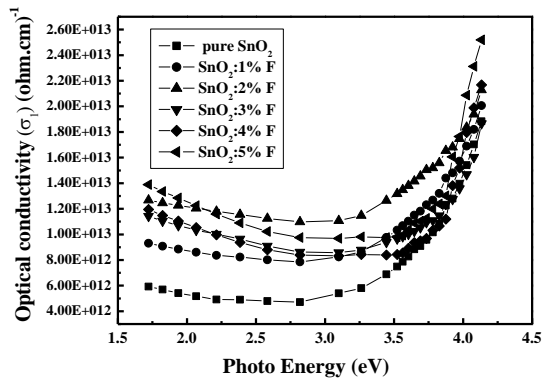
Fig. 12 Variation of Dielectric loss with photo energy for pure and doped samples.

Real and imaginary components of optical conductivity were calculated using the equations (12) and (13) respectively [37].

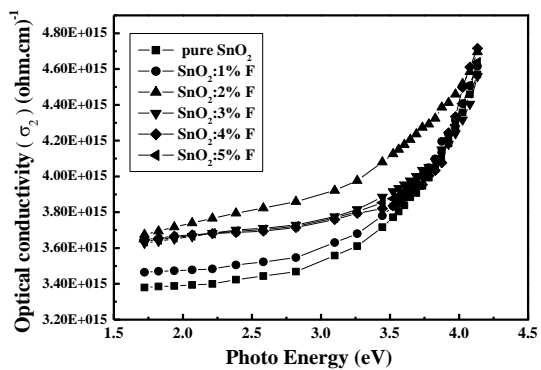
$$\sigma_1 = \omega \epsilon_1 \epsilon_o \dots\dots(13)$$

$$\sigma_2 = \omega \epsilon_2 \epsilon_o \dots\dots(14)$$

and where is the angular frequency, is the permittivity of free space. The spectra of real and imaginary parts of the optical conductivity are shown in Figure 8. It can be seen that both the real and imaginary part increases with increasing the photon energy up to 3.5 eV which can be attributed to excitation of electrons by photon energy [37]. Real part of optical conductivity continue increasing sharply beyond 3.5 eV of photon energy as seen in Figure 8 suggesting strong excitation of the electrons.



( a )



( b )

Fig 13 ( a – b ) Spectra of the real and imaginary part of the optical conductivity of the pure and doped samples.

## Conclusion

From the obtained results of the present work it can be concluded that:-

- 1) The nano particles of SnO<sub>2</sub> thin films with different molar concentrations of F<sup>-1</sup> ions successfully synthesized using well known chemical spray pyrolysis technique.
- 2) The XRD analysis of the prepared thin films established as crystalline structure. The F<sup>-1</sup> concentration enhances the crystalline structure and decreases the intensity of the peak at deposited thin films.
- 3) The prepared thin films have high transmittance in the visible and near IR-regions, thus the SnO<sub>2</sub>:F thin films are convenient as a window for solar cell

## Reverences

[1] R. Kumar, C. Zhou, ACS Nano, 4 (2010) 11  
 [2] M. Adnane, H. Cachet, G. Folcher, S. Hamzaoui, Thin Solid Films, 492 (2005) 240.  
 [3] C. Sima, C. Grigoriu, S. Antohe, Thin Solid Films, 519 (2010) 595.  
 [4] A. Purwanto, H. Widiyandari, D. Hidayat, F. Iskandar, K. Okuyama, Chem. Mater., 21 (2009) 4087.  
 [5] M. Oshima and K. Yoshino, J. Electron. Mater., 39 (2010) 816.  
 [6] Q Zhao, S Wu and D Miao, Adv. Mater. Res., 1043 (2011) 150–151.  
 [7] P. Rajaram, Y. Goswami, S. Rajagopalan, V. Gupta, Materials Letters, 54 (2002) 158.  
 [8] P S Shewale, S I Patil and M D Uplane, Semicond. Sci. Technol., 25 (2010) 115008 .  
 [9] Shadia J. Ikhmayies, International Journal of Materials and Chemistry, 2 (2012) 173-177  
 [10] K. L. Chopra, S. Major and D. K. Pandya, Thin Solid films, 102 (1983) 1-46.  
 [11] W. Siefert, Thin Solid Films, 121 (1984) 275-282.  
 [12] R.N. Bhattacharya, D. Banerjee, R. Padmanabhary, Y. T. Wang, J. Chen, Z. E. Ren, A. M. Hermann, R.D. Blaugher, Supercond. Sci. Technol., 5 (2002) 1288.  
 [13] E. Elengovan, K.Ramamurthi, Journal of Optoelectronics and Advanced Materials, 5 (2003) 45–54.  
 [14]. A.A. Yadava, E.U. Masumdara, A.V. Moholkar, M. Neumann-Spallart, K.Y. Rajpured and C.H. Bhoaled, Journal of Alloys and Compounds, 448 (2009) 350–355.  
 [15] N.F.Habubi, K. A. Mishjal, Z. T. Kasiar, J. of Education College, 2 (2002) 81.  
 [16] X. Li, T. Gessert, C. Dehart, T. Barnes, H. Moutinho, Y. Yan, D. Young, M. Young, J. Perkins, and T. Coutts, Lakewood, Colorado, 520(2001) 3101.  
 [17], L. M. Caicedo, L. C. Moreno, J. W. Sandino, G. Gordillo, Surface Review and Letters, 9 (2002) 1693.  
 [18] S.A. Alnaimi and M.N. AL-Dileamy "Determination of the Optical Constants of Cadmium Stannate ( Cd<sub>2</sub>SnO<sub>4</sub>) films " 3 (2007) 30-39.

application . All films prepared have high values of absorption coefficient ( $\alpha > 10^4 \text{cm}^{-1}$ ) Increasing in energy gap value for the direct, allowed and forbidden transitions by the doping percentage increasing. Increasing in absorptive value by the doping percentage increasing. Decreasing in transmittance value by the doping percentage increasing. Increasing in reflectivity and extinction coefficient values by the doping percentage increasing. Increasing in refractive index value by the doping percentage increasing. Increasing in real and imaginary part of dielectric constant by the doping percentage increasing, but The variation of dielectric loss with photo energy shown decreasing in all films.

[19] Jun Zhang et al, J. Phys. Condense. Matter, 19 (2007) 256.  
 [20] Kodigala Subba Ramaiah, V. Sundara Raja, Applied Surface Science 253 (2006) 1451–1458  
 [21] Demet Tatar and Bahattin Duzgun, Pramana-journal of Phys., 79 (2012) 137-150.  
 [22] M.M. Bagheri-Mohageri and M. Shokooh-Saremi, Semicond.Sci. Technol., 19 (2004) 764.  
 [23] X. C. Yang, Mater. Sci. Eng. B 93, (2002) 249.  
 [24] A A Yadav, E U Masumdar, A V Moholkar, M Neumann-Spallart, K Y Rajpure and C H Bhoale, J. Alloys and Compounds, 448 (2009) 350.  
 [25] N. H. Vasoya, V. K. Lakhani, P. U. Sharma, K. B. Modi, Ravi Kumar and H. H. Joshi J. Phys. : Condens. Matter, 18 (2006) 8063  
 [26] M. M. Bagheri-Mohagheri and M. Shokooh-Saremi, Semicond. Sci. Technol., 19 (2004) 764.  
 [27] A.K. Abass, A.K. Hassen and R.H. Misho, Jappl. Phys, 58 (1985) 1640.  
 [28] Bushra. K.H.al-Maiyaly, I.H. Khudayer, Ayser J.Ibraheim, International Journal of Innovative Research in Science Engineering and Technology, 3 (2014) 8694 – 8700.  
 [29] R. Ferro, J. A. Rodrigucz, Phys. Stat. Sol. (B), 220 (2000) 299.  
 [30] N. F. Habubi, K.A. Mishjal, A.H. Dagir, J. of College of Education, .1 (1993) 5 .  
 [31] B. Thangaraju, P. Kaliannan, Crys Res, Techonol, 35 (2012) 71-75 .  
 [32] M. M. Abdul El- Raheem and Ateyyah M. Al – Baradi, International Journal of Physical Sciences;; 8 (2013) 1570 – 1580.  
 [33] S.K. Al-Ani and C.A. Hogarth, J. Materials science 20 (1985) 2526-2532.  
 [34] P.Nagles, "Electronic transport in Amorphous semiconductors", (1979).  
 [35] Khalid Haneen Abass International Letters of Chemistry, Physics and Astronomy, 6 (2015) 24 – 31.  
 [36] Xu Z-J, Zhang F, Zhang R-J, Yu X, Zhang D-X, Wang Z-Y, et al.. Appl Phys A. 113 (2013) 557–62.  
 [37] Xu J-P, Zhang R-J, Chen Z-H, Wang Z-Y, Zhang F, Yu X,. Nanoscale Res Lett. 9 (2014) 1–6.

## " تحضير أغشية أكسيد القصدير المشوب بفلور بطريقة الرش الكيميائي الحراري "

عبدالسميع فوزي عبدالعزيز البياتي

قسم الفيزياء ، كلية التربية للعلوم الصرفة ، جامعة تكريت ، تكريت ، العراق

## الملخص

في هذا البحث تم تحضير ودراسة الخواص التركيبية والبصرية لأغشية أكسيد القصدير النقي والمشوب بفلور بطريقة الرش الكيميائي الحراري على أرضيات زجاجية بدرجة حرارة  $400^{\circ}\text{C}$ . تم فحص طبيعة تبلور المركبات باستخدام تقنية حيود الأشعة السينية التي أظهرت أن الأغشية متعددة التبلور وان عمليات التشويب بالفلور لاتعطي أي تأثير ملحوظ على التركيب البلوري لأغشية  $\text{Sn}_2\text{O}$ . ان القياسات الكهربائية المستمرة للنماذج تم إيجادها بطريقة ثنائي الأقطاب، إذ تم حسب طاقات التنشيط من رسم العلاقة بين التوصيلية الكهربائية المستمرة كدالة لدرجة الحرارة  $1000 / T$ . أن القيم البصرية المتمثلة بالامتصاصية و الانعكاسية تم تسجيلها عند الأطوال الموجية ( 300 – 1100 ) nm كما تم حساب فجوة الطاقة المباشرة وغير المباشرة المسموحة. كما تم حساب القيم البصرية الأخرى مثل معامل الامتصاص البصري (  $\alpha$  ) ومعامل الخمود (  $K_0$  ) وثابت العزل الكهربائي (  $\epsilon$  ) وخسارة العزل (  $\tan\delta$  ) كدالة لطاقة الفوتون (  $h\nu$  )